Metastability of an immiscible Cu-Mo system calculated from first-principles and a derived *n*-body potential

H. R. Gong, L. T. Kong, and B. X. Liu*
Advanced Materials Laboratory, Department of Materials Science and Engineering, Tsinghua University, Beijing 100084, China
(Received 2 April 2003; revised manuscript received 2 September 2003; published 15 January 2004)

An *ab initio* calculation is performed to predict the structures, lattice constants, and cohesive energies of the metastable $Cu_{75}Mo_{25}$, $Cu_{50}Mo_{50}$, and $Cu_{25}Mo_{75}$ phases. With the aid of an *ab initio* calculation, an *n*-body Cu-Mo potential is derived and proven to be realistic in reproducing some intrinsic properties of the metastable Cu-Mo phases. Based on the Cu-Mo potential, a molecular dynamics simulation reveals that a crystal-to-amorphous transition takes place in a Cu-rich fcc solid solution when the solute concentration reaches/exceeds a critical value of 25 at. % Mo. Moreover, a molecular dynamics simulation also predicts the formation of metastable fcc and bcc Cu-Mo phases and determines the heats of formation of both crystalline and amorphous phases, thus constructing an energy diagram of the Cu-Mo system over the entire composition range. The calculation/simulation results are compared with the experimental observations, and the agreements between them are fairly good.

DOI: 10.1103/PhysRevB.69.024202 PACS number(s): 61.43.Bn

I. INTRODUCTION

During the past decades, a number of metastable alloys were produced by various nonequilibrium techniques, such as mechanical alloying, vapor quenching, ion beam mixing, etc., in many equilibrium immiscible binary metallic systems, which, in many cases, have no any equilibrium alloy phase.[1,2] For instance, metastable fcc and bcc Cu-Fe solid solutions were both obtained by vapor deposition and showed different magnetic properties.[3] Metastable Cu-Cr and Cu-Nb alloys were found to possess a high strength and a high electrical conductivity, and were possible candidates in electrical devices and high-field magnets, respectively.[4,5] As a result, the prospective applications of the metastable alloys have raised much interest for theoretical investigations concerning the metastability of the equilibrium immiscible systems. In this respect, Miedema *et al.* developed, in the mid 1970s, a semiempirical thermodynamic model to predict the metastable alloy phase formation in a semiquantitative manner.[2] Later, based on Miedema *et al.*'s model, Alonso *et al.* developed a semiempirical method to calculate the free energy diagram of the binary metallic systems for understanding the metastable alloy phase formation.[6] Meanwhile, two other powerful means have been employed to study the metastability of binary metallic systems, i.e., a molecular dynamics (MD) simulation for revealing the physical mechanism at an atomistic scale and a first-principles calculation for a theoretical modeling at a depth of the electronic structure of solids. The present work proposes a comprehensive method for studying the metastability of an equilibrium immiscible binary metallic system by combining an *ab initio* calculation and a MD simulation based on a realistic *n*-body potential.

Among the immiscible binary metallic systems, the Cu-Mo system, characterized by a large positive heat of formation ($\Delta H_f = +28$ kJ/mol)[2] has drawn much attention in recent decades.[7–12] For example, in 1985, Dirks and Broek found that vapor-deposited $Cu_{100-x}Mo_x$ thin films exhibited a bcc structure when $30 \leqslant x < 100$ and had an fcc structure when $0 < x \leqslant 20$. They also observed that the electrical resistivity of Cu-Mo alloys increased with the alloy concentration when $0 \leqslant x \leqslant 50$ and decreased when $50 < x \leqslant 100$.[7] Very recently, Djemia *et al.* found that the elastic constants of the ion-beam-sputtered Cu-Mo alloy films laid between those of pure Cu and Mo, and that a hardening of approximately 22% of elastic constants occurred for the $Cu_{30}Mo_{70}$ alloy films after annealing at 760 K.[8] Moreover, Yang and Rockett reported that metastable solid solutions of Cu in Mo containing approximately 30 at. % Cu could provide a significantly enhanced adhesion to the $CuInSe_2$ substrate, resulting in improving the uniformity as well as the performance of the photovoltaic devices.[9] Considering the above background, the immiscible Cu-Mo system is thus selected as a model system for the present study. To the authors' knowledge, there is no realistic *n*-body potential or *ab initio* calculation reported for the Cu-Mo system in the literature. With regard to the construction of an *n*-body Cu-Mo potential, it should be noted that in the equilibrium immiscible Cu-Mo system, there is no equilibrium compound which could provide some physical data for fitting the Cu-Mo cross potential. In this respect, Luzzi *et al.*, in the early 1990s, proposed to perform an *ab initio* calculation for obtaining some physical properties of the metastable Cu_3Bi alloy and the calculated data were used in constructing a Finnis-Sinclair Cu-Bi potential.[13,14] Later, Siegl *et al.* also used this Cu-Bi potential to study atomic structures of the grain boundaries in some Cu-Bi alloys.[15] In the present study, we adopt the same approach to construct an *n*-body Cu-Mo potential. Accordingly, we first perform *ab initio* calculation to predict the structures, lattice constants, and cohesive energies of the possible metastable $Cu_{75}Mo_{25}$, $Cu_{50}Mo_{50}$, and $Cu_{25}Mo_{75}$ phases. Some of the *ab initio* calculated properties, i.e., the properties of the $L1_2$ $Cu_{75}Mo_{25}$ and $B2$ $Cu_{50}Mo_{50}$ phases, are then employed to derive the Cu-Mo cross potential, thus constructing an *n*-body Cu-Mo potential under the framework of an embedded-atom method. Based on the proven realistic

Cu-Mo potential, a MD simulation is conducted to predict the formation of metastable Cu-Mo phases in either crystalline or amorphous structures as well as to determine the heats of formation of the metastable Cu-Mo phases of the system.

II. THEORETICAL AND CHARACTERIZATION METHODS

A. *Ab initio* calculation

The first-principles calculation is based on the well-established Vienna *ab initio* simulation package.[16] The calculations are conducted in a plane-wave basis, using nonlocal Vanderbilt-type ultrasoft pseudopotentials to describe the electron-ion interaction,[17] which allows the use of a moderate cutoff for the construction of the plane-wave basis for the transition metals. In the calculations, the exchange and correlation items are described by the generalized-gradient approximation of Perdew and Wang.[18] The integration in the Brillouin zone is done on special k points determined according to the Monkhorst-Pack scheme.[19]

In the present *ab initio* calculations, we only choose some simple structures for the possible metastable $Cu_{75}Mo_{25}$, $Cu_{50}Mo_{50}$, and $Cu_{25}Mo_{75}$ phases, based on the following considerations. First, for a complicated structure, such as $D0_2$, $D0_{21}$, $L1_a$, etc. Its unit cell contains more atoms than simple structures and frequently requires large computational resources, which are impractical because of the limitation of the calculation capability at present. Second, experimental results signify that the metastable alloy phases are, in many cases, of simple structures, such as fcc, bcc, and hcp structures, rather than complicated ones. The experimental results seem to suggest that a unit cell with a larger size probably requires a larger critical radius and longer time for nucleation and growth, and it is perhaps more likely to be frustrated under the restricted kinetic conditions available in the nonequilibrium producing processes, such as ion beam mixing, vapor deposition, etc. The following fact may lend some support to this argument, i.e., ion irradiation of the $Ni_{50}Mo_{50}$ multilayers resulted in the formation of a metastable hexagonal phase, instead of the most stable equilibrium δ phase,[20] which has an exact stoichiometry of $Ni_{50}Mo_{50}$. The hexagonal phase is a simple structure with two atoms in a unit cell, while the δ phase has been characterized to be a very complicated and ordered orthorhombic structure with 56 atoms in a unit cell.[21] The structural complexity of the δ phase is believed to be the major factor that prevents its formation under an extremely restricted kinetic condition available in the ion irradiation process.[20] Besides, experimental observations signify that the metastable Cu-Mo phases formed so far in the literature are of simple structures, such as bcc and fcc, rather than complicated ones.[7,10–12,22,23]

In particular, the $Cu_{25}Mo_{75}$ phase was found to have a bcc structure in experiments.[22,23] However, there is no such atomic configuration corresponding to the bcc structure of the AB_3 phase in the list of the ordered structures. Consequently, in the present *ab initio* calculation, we adopt the ordered configuration of the bcc structure proposed by Shi *et al.*[24] for the bcc $Cu_{25}Mo_{75}$ phase, and its unit cell is set to contain four atoms.

B. Molecular dynamics simulation

A molecular dynamics simulation is carried out with a Parrinello-Rahman constant pressure scheme and the equations of motion are solved through a fourth-order predictor-corrector algorithm of Gear with a time step of $t=5\times10^{-15}$ s.[25] In the present study, two kinds of simulation models are employed for all the Cu-Mo phases, i.e., an fcc solid solution model, which consists of $7\times7\times7\times4=1372$ atoms, and a bcc solid solution model, which contains $8\times8\times8\times2=1024$ atoms. In all the above simulation models, the [100], [010], and [001] atomic crystal directions are parallel to the x, y, and z axes, respectively, and periodic boundary conditions are adopted in three dimensions. In the fcc (bcc) solid solution models, to obtain a specific chemical stoichiometry of a Cu-Mo alloy phase, a desired number of Cu (Mo) atoms are random substituted by Mo (Cu) atoms in the models. The models are then run at 300 K for adequate MD time steps (usually 100 000 MD time steps) to reach a state, at which the main dynamic parameters, such as the total energy of the model, the volume per atom, etc., do not show any secular variation, i.e., the variations of the parameters are less than 0.1% during 1000 MD time steps.

The process of the structural phase transition is monitored by the projections of the atomic positions, the planar structure factor $S(\mathbf{k})$, the pair-correlation function $g(r)$, and the density profiles of each species along the z direction $\rho_\alpha(z)$. The planar structure factor $S(\mathbf{k})$ is a Fourier transformation of the density to characterize the long-range order in the direction of any vector $\mathbf{k}$, which is a vector of the reciprocal space lattice. Accordingly, the planar structure factor $S=1$ refers to an entirely ordered crystal, while $S=0$ is for a completely disordered state.[26] In the present study, we choose $S(\mathbf{k},\mathbf{z})$, as a specific representative of $S(\mathbf{k})$, to reflect the structural phase transition in each crystallographic plane parallel to the x-y plane. It should be pointed out that the other directions, such as the x or y axis, could also be selected as a representative of $S(\mathbf{k})$, and that the structural change in each direction is reflected by the pair-correlation function in the present study. As one of the main criteria to determine an amorphous structure, the pair-correlation function $g(r)$ is commonly used to identify the structure of a block material by sampling the atoms involved in the block.[27] The density profile $\rho_\alpha(z)$ is calculated to define the position of a single atomic layer, indicating the local structural and compositional properties of the models.[28]

III. RESULTS AND DISCUSSION

A. Prediction of metastable crystalline Cu-Mo phase formation

An *ab initio* calculation is performed to predict the structures, lattice constants, and cohesive energies of some metastable crystalline phases in the Cu-Mo system. In the present study, only three chemical stoichiometries of $Cu_{75}Mo_{25}$, $Cu_{50}Mo_{50}$, and $Cu_{25}Mo_{75}$ are calculated due to the restriction of the currently available calculation method. As mentioned above, only simple structures are selected for the calculation, i.e., the $A15$, $D0_9$, $L1_2$, and $L6_0$ structures for the

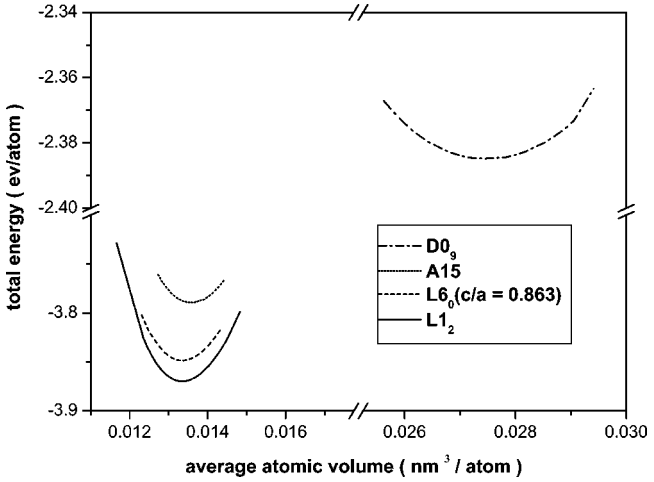

FIG. 1. The *ab initio* calculated total energy vs average atomic volume for the metastable crystalline $Cu_{75}Mo_{25}$ phase in different structures.

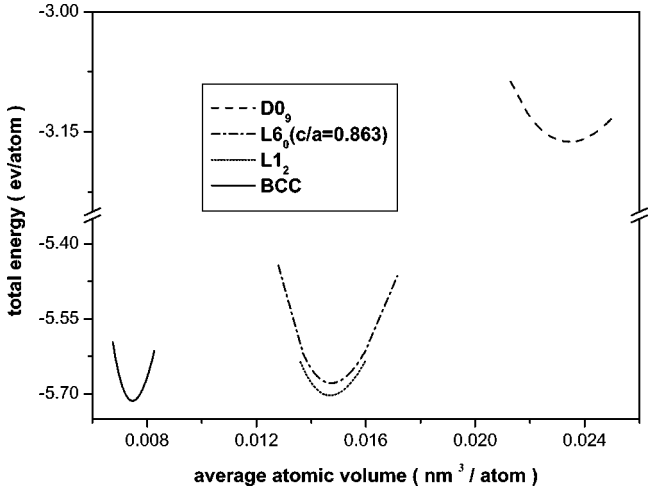

FIG. 3. The *ab initio* calculated total energy vs average atomic volume for the metastable crystalline $Cu_{25}Mo_{75}$ phase in different structures.

$Cu_{75}Mo_{25}$ phase, the $B1$, $B2$, $B3$, and $B17$ structures for the $Cu_{50}Mo_{50}$ phase, and the bcc, $D0_9$, $L1_2$, and $L6_0$ structures for the $Cu_{25}Mo_{75}$ phase. Accordingly, the correlation between the total energy and average atomic volume for the metastable crystalline $Cu_{75}Mo_{25}$, $Cu_{50}Mo_{50}$, and $Cu_{25}Mo_{75}$ phases in different simple structures are obtained and shown in Figs. 1, 2, and 3, respectively. One sees from the figures that the metastable crystalline $Cu_{75}Mo_{25}$ phase in an $L1_2$ structure, the metastable crystalline $Cu_{50}Mo_{50}$ phase in a $B2$ structure, and the metastable crystalline $Cu_{25}Mo_{75}$ phase in a bcc structure have, respectively, the lowest total energy among the four calculated structures and therefore are predicted to likely be formed under appropriate conditions. Correspondingly, the lattice constants of the $L1_2$ $Cu_{75}Mo_{25}$ phase, the $B2$ $Cu_{50}Mo_{50}$ phase, and the bcc $Cu_{25}Mo_{75}$ phase are calculated to be 3.77, 3.03, and 3.10 Å, respectively, and their cohesive energies are calculated to be 3.87, 4.67, and 5.71 eV/atom, respectively.

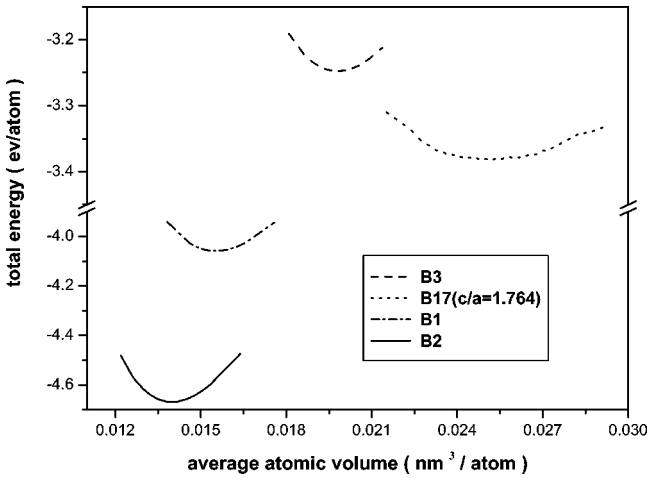

FIG. 2. The *ab initio* calculated total energy vs average atomic volume for the metastable crystalline $Cu_{50}Mo_{50}$ phase in different structures.

From the above calculation results, the heats of formation (ΔH_f) of the $L1_2$ $Cu_{75}Mo_{25}$ phase, the $B2$ $Cu_{50}Mo_{50}$ phase, and the bcc $Cu_{25}Mo_{75}$ phase are derived to be 47.0, 48.7, and 27.3 kJ/mol, respectively. It is noted that the ΔH_f of these metastable crystalline Cu-Mo phases are all large positive values, implying that to obtain these metastable crystalline Cu-Mo phases, nonequilibrium or even far-from-equilibrium materials processing techniques are probably necessary to supply the required positive heats of formation.

It is of interest to testify the above prediction from the *ab initio* calculation by comparing the predicted results with some experimental results observed in the Cu-Mo system. In fact, some metastable crystalline Cu-Mo phases were indeed obtained in experiments by some highly energetic nonequilibrium materials processing techniques.[7,10,22,23,29] For instance, a fcc $Cu_{75}Mo_{25}$ phase, a bcc $Cu_{50}Mo_{50}$ phase, and a bcc $Cu_{25}Mo_{75}$ phase were obtained by vapor deposition,[7] ion beam mixing,[29] magnetron sputtering,[10,22] and ion beam sputtering.[23] Moreover, the lattice constants of the fcc $Cu_{75}Mo_{25}$ phase, the bcc $Cu_{50}Mo_{50}$ phase, and the bcc $Cu_{25}Mo_{75}$ phase determined by diffraction analysis in experiments are about 3.68 Å,[10] 3.05 Å,[22] and 3.114 Å,[23] respectively. Apparently, these experimentally determined lattice constants are in good agreement with the values of 3.77, 3.03, and 3.10 Å, respectively, predicted by the above *ab initio* calculations, as their differences are less than 2.4%. It should be pointed out that such an agreement is excellent, as a measuring error in diffraction analysis could generally be about 3%. In short, the above *ab initio* calculation is a relevant and satisfactory approach for predicting the formation of metastable crystalline phases in the immiscible Cu-Mo system.

B. Construction of an *n*-body Cu-Mo potential

In the present study, we also attempt to investigate the possibility of the metastable Cu-Mo alloy formation through a MD simulation, which has less restriction on the studied

TABLE I. Fitted parameters for the Cu-Cu, Mo-Mo, and Cu-Mo potentials. The three constants, n, r_s, and r_c, are also listed.

Cu-Cu		Mo-Mo		Cu-Mo	
χ	11.134231	χ	7.528924	A	0.393400
α (eV)	0.725977	k_0 (eV)	−0.414269		
β	3.457434	k_1 (eV)	−1.654422	B (Å)	0.083531
r_a (Å)	1.6293656	k_2 (eV)	11.124200		
F_1 (eV)	0.676073	k_3 (eV)	1.712414	C (Å)	0.085263
r_s (Å)	3.7	r_s (Å)	3.2		
r_c (Å)	4.4	r_c (Å)	4.2		
n	0.333333	n	0.57		

chemical stoichiometry than *ab initio* calculation, yet requires a realistic n-body potential constructed prior to the simulation. In deriving the n-body Cu-Mo potential, we employ the embedded-atom method (EAM), which was proposed by Daw and Baskes in 1983 and is based on a density function theory suitable for metals.[30] The method was later successfully developed by Johnson and Oh as well as Cai and Ye to describe the bulk and defect properties of the transition metals in either an fcc or bcc structure.[31,32] For the Cu-Mo system, we adopt the basic function forms of the Cu-Cu and Mo-Mo EAM potentials,[31,32] but with some modifications proposed by the present authors. First, the density function form of Mo-Mo is set to be the same as that of Cu-Cu and it takes a form different from that used in the original work.[31] Second, we adopt a cutoff function proposed by Guellil and Adams,[33] and the cutoff distances (r_s, r_c) are between the second- and third-neighbor distances, whereas the cutoff distance was previously set as $r_{\text{cut}}=1.65a_0$.[32] It should be pointed out that the proposed modifications could improve the precision of the potentials, which will be discussed later. Accordingly, the EAM forms of the Cu-Cu and Mo-Mo potentials are expressed as follows:

$$E_{\text{tot}}=\sum_i F_i(\rho_i)+\frac{1}{2}\sum_{\substack{i,j\\(i\neq j)}}\phi_{ij}(r_{ij}), \tag{1}$$

$$F(\rho)=-F_0\left[1-\ln\left(\frac{\rho}{\rho_e}\right)^n\right]\left(\frac{\rho}{\rho_e}\right)^n+F_1\left(\frac{\rho}{\rho_e}\right), \tag{2}$$

$$\rho_i=\sum_{j\neq i} f(r_{ij}), \tag{3}$$

$$f(r)=f_e\exp[-\chi(r/r_e-1)], \tag{4}$$

$$\phi_{\text{Cu}}(r)=-\alpha[1+\beta(r/r_a-1)]\exp[-\beta(r/r_a-1)], \tag{5}$$

$$\phi_{\text{Mo}}(r)=\begin{cases}\Phi(r)=k_0+k_1(r/r_e-1)+k_2(r/r_e-1)^2\\ \qquad +k_3(r/r_e-1)^3, \qquad r_e\leqslant r\leqslant r_s,\\ \Phi'(r)=\Phi(r)+k_a[(\Phi(r)-\Phi(r_e)](r/r_e-1)^2,\\ \qquad r<r_e,\end{cases} \tag{6}$$

where E_{tot} is the total energy, $F(\rho)$ is the embedding energy, ρ_i is the total electron density at atom i due to all other atoms, $\phi(r_{ij})$ is the pair potential between atom i and j, and $f(r_{ij})$ is the electron density for atom i contributed by atom j. In Eq. (2), F_0, ρ_e, and n are three constants. $F_0=E_c-E_v^f$, in which E_c and E_v^f are the cohesive energy and vacancy formation energy, respectively. The parameter ρ_e represents the host electron density at an equilibrium state. For the Cu-Cu potential, F_1 is an adjustable parameter; while for the Mo-Mo potential, F_1 equals 0. In Eq. (4), r_e is an equilibrium first-neighbor distance, and f_e is a scaling factor determined by the relationship of $f_e=E_c/\Omega$, where Ω is the atomic volume. In the above equations, there are totally five parameters $(\chi,\alpha,\beta,r_a,F_1)$ to be fitted for the Cu-Cu potential and also five parameters (χ,k_0,k_1,k_2,k_3) to be fitted for the Mo-Mo potential.

Having specified the function forms of $F(\rho)$, $f(r)$, and $\phi(r)$, we now turn to describe the fitting process of the Cu-Cu (Mo-Mo) potential. First, some experimental results of pure metal Cu (Mo), i.e., the lattice constant a, the cohesive energy E_c, as well as the elastic constants C_{11}, C_{12}, and C_{44}, are used as input physical data for fitting. Second, the three constants, i.e., n, r_s, and r_c, are set a value, respectively, as follows: the exponential n, to our experience, is set to be around 0.5; the cutoff distances, r_s and r_c, are set to be between the second- and third-neighbor distances, and the value of r_c should be a little greater than that of r_s. The above five potential parameters are then determined by minimizing the root-square deviation between the calculated and experimental data. After each fitting the energy curve of Cu (Mo) are checked and should be similar to that derived from the equation of state of Rose *et al.*[34] Finally, the values of the three constants, n, r_s, and r_c, are changed slightly for a number of times, in order to find a group of optimized parameters, corresponding to the optimized fitting results. After the above fitting procedure and optimization, Table I lists the obtained potential parameters as well as the above three constants and Table II shows the comparison between some physical properties reproduced by the potentials and the experimental values used initially for fitting the Cu-Cu and Mo-Mo potentials. It can be seen from Table II that the fitted Cu-Cu potential shows a better description of pure Cu than that of the original potential[32] and the fitted Mo-Mo potential gives the better results in reproducing some physical proper-

TABLE II. The values of cohesive energy E_c, lattice constant a, bulk modulus, elastic constants, and vacancy formation energy E_v^f of Cu and Mo between calculated and experimental data.

	Cu			Mo		
	Experimental	Cai *et al.*	This work	Experimental	Lee *et al.*	This work
E_c (eV/atom)	3.54[a]	3.52[e]	3.54	3.81[f]		6.81
a (Å)	3.615[b]	3.615[e]	3.615	3.15[b]		3.15
C_{11} (Mbar)	1.70[c]	1.68[e]	1.70	4.647[g]	4.649[h]	4.647
C_{12} (Mbar)	1.225[c]	1.263[e]	1.225	1.615[g]	1.655[h]	1.615
C_{44} (Mbar)	0.758[c]	0.752[e]	0.758	1.089[g]	1.088[h]	1.089
E_v^f (eV)	1.30[d]	1.31[e]	1.30	2.85[g]	3.09[h]	2.85

[a]Reference 35.
[b]Reference 36.
[c]Reference 37.
[d]Reference 38.
[e]Reference 32.
[f]Reference 39.
[g]Reference 40.
[h]Reference 41.

ties of pure Mo than that obtained by Lee *et al.* employing the second nearest-neighbor modified EAM potential.[41]

The Cu-Mo cross potential takes the basic form adopted by Chen *et al.*,[42] yet with some modifications proposed by the present authors, i.e., the substitution of the variable ($r = a + bx$) and the adoption of an assumption ($b = d = f$). Consequently, seven potential parameters in the original form are reduced into three and the function form is simplified into

$$\phi_{\mathrm{CuMo}}(r) = A[\phi_{\mathrm{Cu}}(r+B) + \phi_{\mathrm{Mo}}(r+C)], \tag{7}$$

where r is the distance between Cu and Mo atoms. A, B, and C are three potential parameters to be fitted. Apparently, the above modifications do not change the physical meaning of the original function form. We now present the fitting process of the Cu-Mo cross potential. First, the above fitted parameters of the Cu-Cu and Mo-Mo potentials are used as input constants in fitting of the Cu-Mo cross potential. As there is no any equilibrium alloy phase in the immiscible Cu-Mo system, we use the above *ab initio* calculated lattice constants and cohesive energies of the $L1_2$ $Cu_{75}Mo_{25}$ and $B2$ $Cu_{50}Mo_{50}$ phases for fitting the Cu-Mo cross potential.[13,14,43,44] The above three potential parameters are then determined by minimizing the root-square deviation between *ab initio* calculated data and those from the Cu-Mo potential. Finally, the energy curves of the $Cu_{75}Mo_{25}$ and $Cu_{50}Mo_{50}$ phases are also checked in comparison with those from the equation of state of Rose *et al.*[34] Accordingly, the fitted parameters are obtained and also listed in Table I. The fitted results as well as the original fitting data from *ab initio* calculation are all displayed in Table III. One sees clearly from Table III that the fitted lattice constants of the $Cu_{75}Mo_{25}$ and $Cu_{50}Mo_{50}$ phases are 3.73 and 3.04 Å, respectively, which are in good agreement with the values of 3.77 and 3.03 Å acquired from *ab initio* calculations, and that the fitted cohesive energies of the $Cu_{75}Mo_{25}$ and $Cu_{50}Mo_{50}$ phases are 3.81 and 4.52 eV/atom, respectively, which are also compatible with the *ab initio* calculated values of 3.87 and 4.67 eV/atom, as their differences are less than 3.3%. In short, the Cu-Mo cross potential works quite well for a satisfactory description for some metastable crystalline phases in the equilibrium immiscible Cu-Mo system.

We now turn to validate the newly constructed Cu-Mo potential. First, we use both an *ab initio* calculation and the Cu-Mo potential to derive some elastic constants of $L1_2$ $Cu_{75}Mo_{25}$ and $B2$ $Cu_{50}Mo_{50}$ phases, and these values from two different methods are compared. Second, the energies of the $Cu_{75}Mo_{25}$ and $Cu_{50}Mo_{50}$ phases in other possible simple structures are also calculated from the Cu-Mo potential, respectively, and are compared with those from *ab initio* calculations. Third, MD simulations using the Cu-Mo potential are conducted to derive some physical properties of the metastable bcc $Cu_{25}Mo_{75}$ and $Cu_{30}Mo_{70}$ phases, and the de-

TABLE III. Comparison of some physical properties derived from *ab initio* calculation and the Cu-Mo potential for the metastable $L1_2$ $Cu_{75}Mo_{25}$ and $B2$ $Cu_{50}Mo_{50}$ phases. ΔE_1, ΔE_2, and ΔE_3 are the energy differences of the $Cu_{75}Mo_{25}$ phase in the $L6_0$, $A15$, and $D0_9$ structures, with respect to it in the $L1_2$ structure, respectively. ΔE_4, ΔE_5, and ΔE_6 are the energy differences of the $Cu_{50}Mo_{50}$ phase in the $B1$, $B3$, and $B17$ structures, with respect to it in the $B2$ structure, respectively.

	$Cu_{75}Mo_{25}$		$Cu_{50}Mo_{50}$	
	Ab initio calculation	Cu-Mo potential	*Ab initio* calculation	Cu-Mo potential
a (Å)	3.77	3.73	3.03	3.04
E_c (eV/atom)	3.87	3.81	4.67	4.52
B (Mbar)	1.62	1.42	2.02	2.09
C_{11} (Mbar)	1.675	1.453	0.747	0.653
C_{12} (Mbar)	1.596	1.418	2.660	2.809
C_{44} (Mbar)	0.327	0.367	1.355	1.073
ΔE_1 (eV/atom)	0.02	0.01		
ΔE_2 (eV/atom)	0.08	0.14		
ΔE_3 (eV/atom)	1.48	0.96		
ΔE_4 (eV/atom)			0.62	0.66
ΔE_5 (eV/atom)			0.81	1.11
ΔE_6 (eV/atom)			1.29	1.32

rived data are compared with those from *ab initio* calculation and experiments. Finally, the ultimate and important validation of the Cu-Mo potential is to compare the metastability revealed by the present potential and the experimental observations reported so far, and the good agreements between them will be shown in Secs. III C and III D.

Applying the method proposed by Mehl *et al.*,[45] we perform an *ab initio* calculation to derive the elastic constants of $L1_2$ $Cu_{75}Mo_{25}$ and $B2$ $Cu_{50}Mo_{50}$ phases. The main idea is presented as follows: we apply small strains to the equilibrium lattice, determine the resulting change in the total energy, and from this information, then deduce the elastic constants through fitting.[45] In addition, using the present Cu-Mo potential, we also calculate the elastic constants of $L1_2$ $Cu_{75}Mo_{25}$ and $B2$ $Cu_{50}Mo_{50}$ phases under the expressions of the elastic constants proposed by Chantasiriwan and Milstein.[46] Accordingly, the calculated results from *ab initio* calculation and the derived Cu-Mo potential are listed in Table III. Generally speaking, the calculated results from two methods are in reasonable agreement with each other. For instance, one sees that the shear modulus, C_{44}, of the $L1_2$ $Cu_{75}Mo_{25}$ phase derived from the Cu-Mo potential is 0.367, which is in good agreement with the value of 0.327 calculated from *ab initio* calculations, and that the bulk modulus, *B*, of the $B2$ $Cu_{50}Mo_{50}$ phase from the Cu-Mo potential is 2.09, which matches well with the *ab initio* calculated value of 2.02. It is noticed that for other elastic constants, there are some differences between the values from the derived potential and *ab initio* calculations, implying that an empirical potential may not be perfect in some aspects.

Meanwhile, we use the Cu-Mo potential to calculate the minimum total energies of the $Cu_{75}Mo_{25}$ phase in $D0_9$, $A15$, and $L6_0$ structures, respectively, and of the $Cu_{50}Mo_{50}$ phase in $B1$, $B3$, and $B17$ structures, respectively. The energy differences of these values with respect to the minimum total energies of $L1_2$ $Cu_{75}Mo_{25}$ and $B2$ $Cu_{50}Mo_{50}$ phases respectively, are shown in Table III. In comparison, the structural energy differences taken at the minima of the energy curves in Figs. 1 and 2 are also calculated and listed in Table III. It can be seen clearly from the table that the Cu-Mo potential is able to reproduce the correct verdict predicted by the above *ab initio* calculation, i.e., the $L1_2$ $Cu_{75}Mo_{25}$ and $B2$ $Cu_{50}Mo_{50}$ phases have the lowest total energies among the calculated simple structures, respectively. It can also be seen that the energy sequences for the $Cu_{75}Mo_{25}$ and $Cu_{50}Mo_{50}$ phases in different structures shown in Figs. 1 and 2 can exactly be reproduced by the present Cu-Mo potential, and that the values of the structural energy differences from the Cu-Mo potential are also compatible with those from *ab initio* calculations. In short, the Cu-Mo potential is quite relevant to reflect the structural energy differences of the $Cu_{75}Mo_{25}$ and $Cu_{50}Mo_{50}$ phases.

We now further validate the Cu-Mo potential by performing a MD simulation to calculate some physical properties of the metastable $Cu_{25}Mo_{75}$ and $Cu_{30}Mo_{70}$ phases. In the simulation, the bcc $Cu_{25}Mo_{75}$ solid solution model is employed and the simulation results show that the solid solution could retain its bcc structure upon annealing at 300 K. Accordingly, some physical properties of the $Cu_{25}Mo_{75}$ phase are calculated and listed in Table IV. One sees clearly from the table that the cohesive energies derived from the MD simulation and *ab initio* calculation match well with each other, as the difference is only about 1.6%. Moreover, the lattice constant of the bcc $Cu_{25}Mo_{75}$ phase is deduced to be 3.13 Å, which is in excellent agreement with the value of 3.10 Å predicted by the *ab initio* calculation as well as with the experimentally determined value of 3.114 Å for the $Cu_{25}Mo_{75}$ alloy obtained by ion beam sputtering.[23] It should be emphasized that the related properties of the $Cu_{25}Mo_{75}$ phase obtained by an *ab initio* calculation were not used in fitting the Cu-Mo cross potential. Consequently, such good agreements among *ab initio* calculation, MD simulation, and experiments could also lend some support to the relevance of the constructed Cu-Mo potential. A similar MD simulation is also conducted with the bcc $Cu_{30}Mo_{70}$ solid solution model and the results as well as some experimental observations are also listed in Table IV. The MD simulation shows that the solid solution could also retain a bcc structure upon annealing at 300 K. Interestingly, a bcc $Cu_{30}Mo_{70}$ alloy was indeed obtained by vapor deposition,[7] magnetron sputtering,[22] and ion beam sputtering.[23] The lattice constant of the alloy determined by the present MD simulation is 3.12 Å, which matches well with the experimental value of 3.114 Å.[23]

TABLE IV. The structure, lattice constant *a*, and cohesive energy E_c of the metastable $Cu_{25}Mo_{75}$ and $Cu_{30}Mo_{70}$ phases derived from calculation/simulation and experiments, respectively.

Phases	Method	Structure	*a* (Å)	E_c (eV/atom)
$Cu_{25}Mo_{75}$	*Ab initio* calculation	bcc	3.10	5.71
	MD simulation	bcc	3.13	5.64
	Experimental	bcc[a,b]	3.114[b]	
$Cu_{30}Mo_{70}$	MD simulation	bcc	3.12	5.35
	Experimental	bcc[a,b,c]	~3.114[b]	

[a]Reference 22.
[b]Reference 23.
[c]Reference 7.

C. Prediction of amorphous Cu-Mo phase formation

It is known that a MD simulation with an *n*-body potential is a powerful means to study the detailed process of the crystal-to-amorphous transition at an atomistic scale and that using a solid solution model, simulation is able to determine the critical solubility for the transition by comparing the energy levels of the solid solution versus its disordered counterpart as a function of composition.[1,47] In the present study, we first perform the simulation with a Cu-rich fcc Cu-Mo solid solution model to examine its stability while gradually increasing the Mo concentration in the solid solution. The simulation results show that when the solute concentration equals/exceeds a critical value of 25 at. % Mo, the Cu-rich fcc solid solution becomes unstable and turns into amorphous. Figure 4 displays four sets of partial and total pair-correlation functions for the Cu-rich fcc solid solutions with four Mo solute concentrations after annealing at 300 K for 100 000 MD time steps, respectively. It can be seen from the

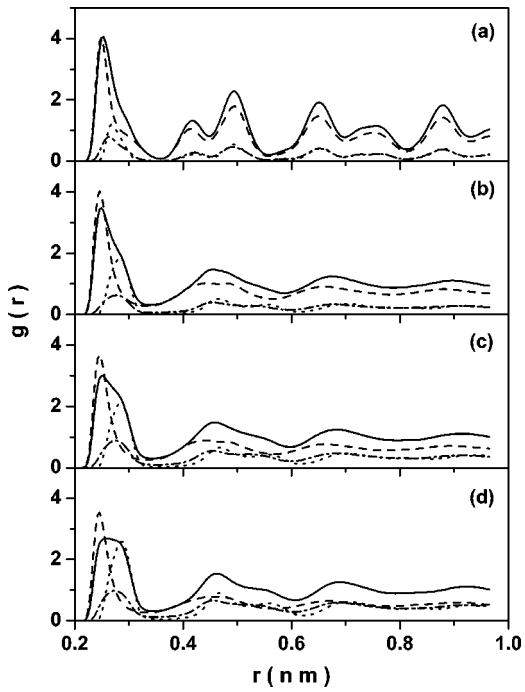

FIG. 4. Partial and total pair correlation functions of the Cu-based solid solution after annealing at 300 K for 100 000 MD time steps. The Mo solute concentrations are (a) 20 at. %, (b) 25 at. %, (c) 35 at. %, and (d) 50 at. %. The solid line is for total $g(r)$, dashed line is for Cu-Cu partial $g(r)$, the dotted line is for Mo-Mo partial $g(r)$, and the dash-dotted line is for Cu-Mo partial $g(r)$.

figure that the $Cu_{75}Mo_{25}$, $Cu_{65}Mo_{35}$, and $Cu_{50}Mo_{50}$ solid solutions all turn into amorphous states, whereas the $Cu_{80}Mo_{20}$ solid solution retains a crystalline structure. It is of interest to note that the above simulation results are in good agreement with the previously reported experimental observations. For instance, Chen and Liu reported that an amorphous alloy was obtained by ion beam mixing in the $Cu_{75}Mo_{25}$ multilayered sample and that crystalline structures remained in the $Cu_{83}Mo_{17}$ multilayered sample under similar experimental conditions.[29,48] Such an agreement between the present simulation results and the experimental observations concerning the amorphous phase formation also supports the argument that the constructed Cu-Mo potential is realistic.

The MD simulation also reveals that the total energies of a fcc $Cu_{75}Mo_{25}$ solid solution and an amorphous $Cu_{75}Mo_{25}$ phase are -3.89 and -3.97 eV/atom, respectively. One sees that the fcc $Cu_{75}Mo_{25}$ solid solution should become amorphous upon thermal annealing, as its energy is higher than that of the amorphous counterpart, and this transition is indeed observed in the above MD simulation. Incidentally, there is another metastable crystalline $Cu_{75}Mo_{25}$ phase, i.e., an $L1_2$ ordered structure, predicted by the above *ab initio* calculation. Accordingly, the total energy of the $L1_2$ $Cu_{75}Mo_{25}$ phase deduced from the MD simulation is -3.81 eV/atom, which is also higher than that of the amorphous state. It is, therefore, predicted that such an energy difference may drive the $L1_2$ structure into a disordered state. To testify the prediction, MD simulation is conducted by using a simulation model in an $L1_2$ structure and the simulation results do confirm that the $L1_2$ structure turns into a disordered state upon annealing at 300 K. It should be noted that the total energies described in this section are negatives of the cohesive energies shown in Tables II and III, and they will be compared in Sec. III D.

D. Construction of the energy diagram of the Cu-Mo system

In the above paragraphs, we have discussed the formation of both metastable crystalline and amorphous Cu-Mo phases. It should be pointed out that the $L1_2$, $B2$, fcc, bcc, and amorphous structures of the $Cu_{100-x}Mo_x$ phase are all metastable states, and that the stable state of the $Cu_{100-x}Mo_x$ phase should be the corresponding mechanical mixture of $(100-x)$% Cu atoms plus x% Mo atoms. We, therefore, conduct MD simulations to compare the energies of the Cu-Mo phases in different states. As the first typical example, the total energies of the $Cu_{75}Mo_{25}$ phase are calculated and the energy sequence is:

$L1_2$ (-3.80 eV/atom) $\rightarrow$ bcc solution (-3.88 eV/atom) $\rightarrow$ fcc solution (-3.89 eV/atom)$\rightarrow$amorphous (-3.97 eV/atom)$\rightarrow$mechanical mixture (-4.36 eV/atom).

One sees that the metastable crystalline $L1_2$, bcc, and fcc structures all have higher energies than the amorphous phase. In other words, an amorphous $Cu_{75}Mo_{25}$ alloy is more likely to be formed than the metastable crystalline phases upon suitable conditions and, as mentioned above, it was indeed obtained in the $Cu_{75}Mo_{25}$ multilayers upon ion beam mixing.[29] As another typical example, the total energies of the $Cu_{50}Mo_{50}$ phase in the different states are also calculated through a MD simulation and a similar energy sequence is obtained as follows:

$B2$ (-4.52 eV/atom)$\rightarrow$fcc solution (-4.57 eV/atom) $\rightarrow$bcc solution (-4.60 eV/atom)$\rightarrow$amorphous (-4.65 eV/atom)$\rightarrow$mechanical mixture (-5.18 eV/atom).

Moreover, we perform MD simulations to determine the energies of the fcc and bcc Cu-Mo phases over the entire composition range as well as the energies of some amorphous phases. In comparison, the energies of the corresponding stable states, i.e., the mechanical mixture of pure Cu and Mo, are also calculated. Consequently, an energy diagram for the $Cu_{100-x}Mo_x$ phases is obtained and shown in Fig. 5. Apparently, all the fcc and bcc phases have higher energies than the mechanical mixtures, and the energies of the amorphous phases are between those of the bcc/fcc phases and mechanical mixtures when $25 \leqslant x \leqslant 50$. Moreover, the bcc $Cu_{100-x}Mo_x$ phase has lower energy than the fcc phase when $30 \leqslant x < 100$, while the fcc phases are more stable than the bcc phases when $0 < x \leqslant 25$. Interestingly, there have been some experimental observations regarding the energy sequences of the fcc and bcc Cu-Mo phases. For instance, Dirk and Broek found that the vapor-deposited Cu-Mo thin films exhibited a bcc structure when $30 \leqslant x < 100$ and had an fcc structure when $0 < x \leqslant 20$.[7] In addition, Xiao *et al.* observed that the Cu-Mo thin films prepared by magnetron sputtering exhibited fcc and bcc structures when $0 < x \leqslant 20$ and $40 \leqslant x < 100$, respectively.[22] It should be pointed out that these experimental observations are quite consistent with the present simulation results, implying the calculated energy diagram,

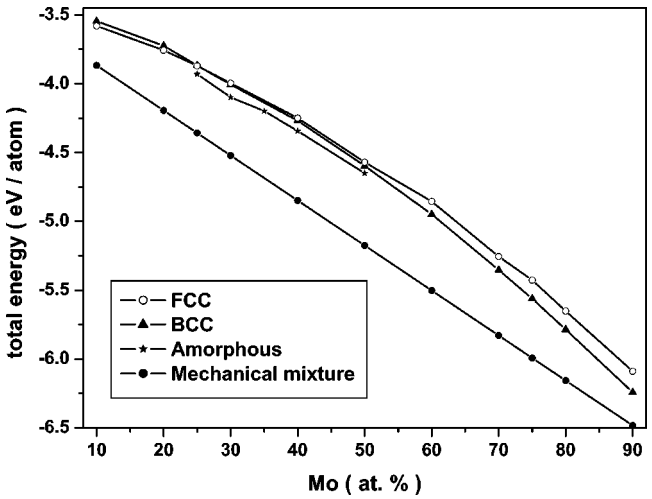

FIG. 5. The calculated results of the total energy vs the Mo compositions for the Cu-Mo phases in different structures.

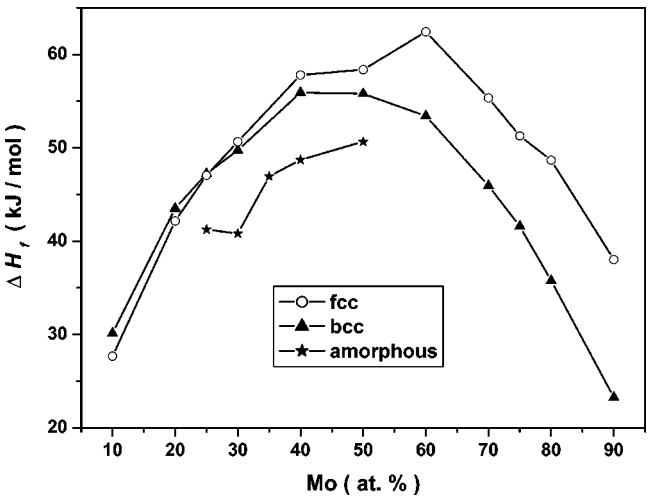

FIG. 6. The MD simulation results of the heat of formation (ΔH_f) vs the Mo compositions for the metastable fcc, bcc, and amorphous Cu-Mo phases, respectively.

determined directly by the Cu-Mo potential through a MD simulation, is of relevance, which in turn also confirms the validation of the newly constructed Cu-Mo potential.

Incidentally, we also calculate the heats of formation (ΔH_f) of the metastable Cu-Mo phases over the entire composition range. Figure 6 shows the calculated values of ΔH_f versus the Mo concentration for the metastable fcc, bcc and amorphous $Cu_{100-x}Mo_x$ phases, respectively. One sees clearly that the bcc structure is more likely formed than the fcc structure in a Mo concentration of $30 \leqslant x < 100$ and the fcc structure is energetically preferred within a concentration range of $0 < x \leqslant 25$, and that an amorphous state has lower ΔH_f than its fcc or bcc counterpart in a concentration range of $25 \leqslant x \leqslant 50$. It should be noted that the sequence of the ΔH_f for various metastable phases shown in Fig. 6 gives a further description of the metastability of the Cu-Mo system revealed by Fig. 5, and is also in good agreement with the experimental observations reported so far in the literature.[7,22]

IV. CONCLUSION

(1) We have shown that combining the first-principles calculation and MD simulation with a proven realistic *n*-body potential is a feasible approach to study the metastability of the highly immiscible Cu-Mo system.

(2) An *ab initio* calculation is able to predict the structures, lattice constants, and cohesive energies of metastable crystalline $Cu_{75}Mo_{25}$, $Cu_{50}Mo_{50}$, and $Cu_{25}Mo_{75}$ phases. The predicted structures and lattice constants are in good agreement with the experimental observations reported so far in the literature.

(3) Through fitting to some *ab initio* calculated properties, an EAM *n*-body Cu-Mo potential is constructed and is able to reproduce some physical properties of the metastable Cu-Mo phases, as well as to reflect the metastability of the Cu-Mo system.

(4) Applying the derived Cu-Mo potential, a MD simulation reveals that 25 at.% Mo is the critical composition to trigger the crystal-to-amorphous transition in the Cu-rich Cu-Mo solid solutions.

(5) The MD simulation is also able to determine the heats of formation of the metastable $Cu_{100-x}Mo_x$ phases in various possible structures, thus obtaining an energy diagram, from which an energetically preferred structure at a specific stoichiometry can be predicted.

ACKNOWLEDGMENTS

The authors are grateful to the financial support from the National Natural Science Foundation of China, The Ministry of Science and Technology of China (G20000672), as well as from Tsinghua University.

*Author to whom correspondence should be addressed. Also at State Key Laboratory of Solid-State Microstructures, Nanjing University, Nanjing 210008, China. Electronic mail: dmslbx @tsinghua.edu.cn

[1] B. X. Liu, W. S. Lai, and Q. Zhang, Mater. Sci. Eng., R. **29**, 1 (2000).

[2] F. R. deBoer, R. Boom, W. C. M. Mattens, A. R. Miedema, and A. K. Niessen, *Cohesion in Metals: Transition Metal Alloys* (North-Holland, Amsterdam, 1989).

[3] E. F. Kneller, J. Appl. Phys. **35**, 2210 (1964).

[4] M. J. Tenwick and H. A. Davies, Mater. Sci. Eng. **98**, 543 (1988).

[5] T. E. Mitchell, Y. C. Lu, A. J. Griffin Jr., M. Nastasi, and H. Kung, J. Am. Ceram. Soc. **80**, 1673 (1997).

[6] J. A. Alonso, L. J. Gallego, and J. A. Simozar, Nuovo Cimento **12**, 587 (1990).

[7] A. G. Dirks and J. J. Van den Broek, J. Vac. Sci. Technol. A **3**, 2618 (1985).

[8] P. Djemia, F. Ganot, P. Moch, V. Branger, and P. Goudeau, J. Appl. Phys. **90**, 756 (2001).

[9] L.-Chung Yang and A. Rockett, J. Appl. Phys. **75**, 1185 (1994).

[10] J. P. Chu and T. N. Lin, J. Appl. Phys. **85**, 6462 (1999).

[11] G. Ramanath, H. Z. Xiao, L. C. Yang, A. Rockett, and L. H.

Allen, J. Appl. Phys. **78**, 2435 (1995).
[12] O. Alvarez-Fregoso, S. López, J. A. Juárez-Islas, M. García, E. Martínez, M. A. Alvarez-Pérez, J. Ch. Ramírez, and S. Granados, Phys. Status Solidi B **220**, 575 (2000).
[13] D. E. Luzzi, M. Yan, M. Šob, and V. Vitek, Phys. Rev. Lett. **67**, 1894 (1991).
[14] M. Yan, M. Šob, D. E. Luzzi, V. Vitek, G. J. Ackland, M. Methfessel, and C. O. Rodriguez, Phys. Rev. B **47**, 5571 (1993).
[15] R. Siegl, M. Yan, and V. Vitek, Model. Simul. Mater. Sci. Eng. **5**, 105 (1997).
[16] G. Kresse and J. Hafner, Phys. Rev. B **47**, 558 (1993).
[17] D. Vanderbilt, Phys. Rev. B **41**, 7892 (1990).
[18] J. Perdew and Y. Wang, Phys. Rev. B **45**, 13 244 (1992).
[19] H. J. Monkhorst and J. D. Pack, Phys. Rev. B **13**, 5188 (1976).
[20] B. X. Liu, L. J. Huang, K. Tao, C. H. Shang, and H-D. Li, Phys. Rev. Lett. **59**, 745 (1987).
[21] C. B. Shoemaker and D. P. Shoemaker, J. Appl. Crystallogr. **16**, 997 (1963).
[22] H. Z. Xiao, L.-Chung Yang, S. L. Lai, Z. Ma, and A. Rockett, Scr. Metall. Mater. **32**, 353 (1995).
[23] Ph. Goudeau, J. Mimault, Th. Girardeau, K. Reklaoui, O. Proux, and V. Branger, Thin Solid Films **275**, 25 (1996).
[24] Y. S. Shi, D. Qian, G. S. Gong, X. F. Jin, and D. S. Wang, Phys. Rev. B **65**, 172410 (2002).
[25] M. Parrinello and A. Rahman, J. Appl. Phys. **52**, 7182 (1981).
[26] S. R. Phillpot, S. Yip, and D. Wolf, Comput. Phys. **3**, 20 (1989).
[27] Y. Waseda, *The Structure of Non-Crystalline Materials: Liquid and Amorphous Solids* (McGraw-Hill, New York, 1980).
[28] V. Rosato, G. Ciccotti, and V. Pontikis, Phys. Rev. B **33**, 1860 (1986).
[29] Y. G. Chen and B. X. Liu, J. Appl. Phys. **82**, 3815 (1997).
[30] M. S. Daw and I. Baskes, Phys. Rev. Lett. **50**, 1285 (1983).
[31] R. A. Johnson and D. J. Oh, J. Mater. Res. **4**, 1195 (1989).
[32] J. Cai and Y. Y. Ye, Phys. Rev. B **54**, 8398 (1997).
[33] A. M. Guellil and J. B. Adams, J. Mater. Res. **7**, 639 (1992).
[34] J. H. Rose, J. R. Smith, F. Guinea, and J. Ferrante, Phys. Rev. B **29**, 2963 (1984).
[35] *Metal Reference Book*, 5th ed., edited by C. J. Smith (Butterworths, London, 1976).
[36] C. Kittel, *Introduction to Solid-State Physics*, 4th ed. (Wiley, New York, 1971).
[37] G. Simmons and H. Wang, *Single Crystal Elastic Constants and Calculated Aggregate Properties: A Handbook*, 2nd ed. (MIT, Cambridge, MA, 1971).
[38] R. W. Balluffi, J. Nucl. Mater. **69&70**, 240 (1978).
[39] *American Institute of Physics Handbook* (McGraw-Hill, New York, 1957).
[40] P. Bujard, Ph.D. thesis, University of Geneva, 1982.
[41] B. J. Lee, M. I. Bakes, H. Kim, and Y. K. Cho, Phys. Rev. B **64**, 184102 (2001).
[42] J. K. Chen, D. Farkas, and W. T. Reynolds Jr. Acta Mater. **45**, 4415 (1997).
[43] F. Ercolessi and J. B. Adams, Europhys. Lett. **26**, 583 (1994).
[44] H. R. Gong, L. T. Kong, W. S. Lai, and B. X. Liu, Phys. Rev. B **66**, 104204 (2002).
[45] M. J. Mehl, J. E. Osburn, D. A. Papaconstantopoulos, and B. M. Klein, Phys. Rev. B **41**, 10 311 (1990).
[46] S. Chantasiriwan and F. Milstein, Phys. Rev. B **53**, 14 080 (1996).
[47] B. X. Liu, W. S. Lai, and Z. J. Zhang, Adv. Phys. **50**, 367 (2001).
[48] Y. G. Chen and B. X. Liu, J. Alloys Compd. **261**, 217 (1997).